Phase-separation dynamics of a ternary mixture coupled with reversible chemical reaction

Chaohui Tong and Yuliang Yang[a)]
Department of Macromolecular Science, Key Lab of Molecular Engineering of Polymers, SMEC, Fudan University, Shanghai 200433, China

(Received 27 July 2001; accepted 15 October 2001)

The phase-separation dynamics of a ternary mixture (A, B and C) coupled with a reversible chemical reaction between the two constituents A and B is presented. It is demonstrated that the free-energy functional form of time-dependent-Ginzburg-Landau equation describing the phase-separation dynamics of the ternary mixture coupled with a reversible chemical reaction is similar to that of the mixture composed of a block copolymer and a homopolymer. Our simulation study reveals that for the case of equal forward and backward reaction rates, the lamellar thickness scales with the reaction rate constant as a single power law $\lambda_L \sim \Gamma^{-0.22}$, regardless of high or low reaction rate regimes. This study sheds insight to the unique features of the involvement of chemical reaction in the phase separation of the ternary mixture. If chemical reaction and phase separation take place simultaneously, the different pattern evolutions at high and low reaction rate constants are originated from the balance between the domain coarsening due to phase separation and the breakup of the continuous phase due to the chemical conversion. The different pattern evolution at high and low reaction rate constants when chemical reaction lags behind phase separation can be interpreted in terms of the discrepancy between the domain sizes at the time step immediately before the turning on of the chemical reaction and the inherent lamellar thickness. It is also pointed out that the crossover of the ternary mixture from one phase region to another, due to the concentration change between A and B, might generate interesting steady-state domain patterns. © *2002 American Institute of Physics.* [DOI: 10.1063/1.1425820]

I. INTRODUCTION

Phase-separation dynamics of binary mixtures such as polymer blends has been intensively studied and the underlying physics is well understood.[1,2] In the early stage of phase separation, the concentration fluctuation grows exponentially for longer wavelength modes above the cutoff wavelength, resulting in the formation of two coexisting phases. As the phase separation further evolves, this pattern slowly coarsens and eventually transforms into two macroscopic phases, separated by an interfacial boundary region.

In real world, phase separation of polymer blends usually proceeds under the presence of an external field such as shear flow, temperature gradient, or chemical reaction.[3–10] The study of phase separation of polymer blends accompanied by chemical reaction is very important from both industrial and theoretical points of view. Reactive blending and reaction injection molding are two important industrial processes, which involve chemical reaction coupled-phase separation. Experimentally, phase separation of binary polymer blends under photo-cross-linking reaction has been extensively investigated by Tran-Cong and fascinating patterns are observed in his studies.[11–14] Over the last several decades, a few theoretical studies have investigated the spinodal decomposition coupled with chemical reaction. Huberman pioneered in this field and examined the effects of chemical reaction upon spinodal decomposition.[15] He predicted that chemical reaction may narrow the band of unstable modes and more importantly introduce a lower cutoff wave number, below which all modes, and in particular, the mode of zero wave number, are stable. More recent theoretical and simulation works support this prediction that chemical reaction may suppress the phase separation and confine the phase-separated domains to microscopic length scale.[16–19]

The chemical reaction investigated in most of the theoretical and simulation studies is the isomerization reaction between the two constituents in the binary mixture:

$$A \underset{\Gamma_2}{\overset{\Gamma_1}{\rightleftarrows}} B. \tag{1.1}$$

The reaction term in time-dependent Ginzburg-Landau (TDGL) equation describing the phase dynamics of binary mixture coupled with reversible reaction (1.1) represents the long-range repulsion, which competes with the short-range attractive interaction and results in the formation of stable periodic structures. It has been pointed out that the forms of TDGL equations for describing the phase separation of both binary mixture, coupled with reversible chemical reaction and block copolymer, are identical.[16–19] However, there are some inherent differences between these two systems.[20,21] In block copolymer, the long-range repulsion originates from the connectivity of the two blocks by chemical bond. The coefficient in the long-range interaction term is determined by the block length of the copolymer, which is an intrinsic parameter of the copolymer. On the other hand, the same

a)Author to whom all correspondence should be addressed.

coefficient involved in reversible chemical reaction is an external parameter and can be varied by changing the reaction rate constants. Also the chemical reaction could be turned on after macrophase separation proceeds first, which might generate interesting steady-state patterns that could not be observed in a block copolymer system. Moreover, the spatial averaged volume fraction is defined by the block ratio and is constant throughout the phase-separation evolution of block copolymer. While in chemical reaction coupled-phase separation, the spatial averaged volume fraction at steady state is determined by the relative amplitude of reaction rates of forward and backward reaction. More importantly, the spatial averaged volume fraction at chemical equilibrium is not necessarily equal to the initial value. Motoyama has carefully investigated the effect of concentration relaxation from initial state to equilibrium state on phase separation and observed interesting steady-state patterns in these systems.[21]

While phase separation has been extensively studied in binary systems, very few studies exist for ternary mixtures. The morphology and dynamics of ternary mixture are more complex than those of binary mixture, and the ternary mixture can phase separate into two or three phases.[22,23]

We are interested in the dynamics of phase separation of multicomponent mixture coupled with more complex reaction than the isomerization reaction in binary mixture, such as the Schlogl reaction model,[24] which involves nonlinear chemical reaction and belongs to a reaction-diffusion problem.

$$C \underset{\Gamma_2}{\overset{\Gamma_1}{\rightleftarrows}} A \qquad 2A + B \underset{\Gamma_4}{\overset{\Gamma_3}{\rightleftarrows}} 3A. \tag{1.2}$$

As an initial step, we emphasize on the study of phase separation of ternary mixture coupled with reversible reaction Eq. (1.1) between A and B, in which C does not participate. As the phase separation of a binary mixture coupled with a reversible chemical reaction is similar to that of a block copolymer, we conjecture that the phase-separation dynamics of ternary mixture, coupled with a reversible chemical reaction between the two constituents, should be similar to that of a mixture composed of a block copolymer and a homopolymer.

II. THE MODEL EQUATIONS AND SIMULATION SCHEME

The Flory–Huggins free energy for the ternary mixture can be written as[22]

$$\begin{aligned} f(\varphi_A,\varphi_B,\varphi_C) = {} & \frac{1}{N}\varphi_A \ln(\varphi_A) \\ & + \frac{1}{N}\varphi_B \ln(\varphi_B) + \frac{1}{N}\varphi_C \ln(\varphi_C) \\ & + \chi_{AB}\varphi_A\varphi_B + \chi_{AC}\varphi_A\varphi_C + \chi_{BC}\varphi_B\varphi_C, \end{aligned} \tag{2.1}$$

where φ_A, φ_B and φ_C are the volume fractions of species A, B, and C, respectively; N_A, N_B, and N_C are the chain lengths of A, B, and C, respectively. For simplicity, N_A, N_B, and N_C are set equal. χ_{ij} is the interaction parameter between the segment i and j, $i,j=A$, B, and C. In this ternary mixture, under the incompressible condition, only two of the local volume fractions are independent. Two order parameters, η and ϕ, are defined as

$$\phi = \varphi_A - \varphi_B, \quad \eta = \varphi_A + \varphi_B - \psi_C, \tag{2.2}$$

where ψ_C is the critical composition of the phase diagram for the phase separation between C and A/B.

By expanding the Flory–Huggins free energy according to the order parameters η and ϕ defined in Eq. (2.2), we obtain

$$\begin{aligned} f(\eta,\phi) \approx {} & \left(\frac{\chi_{AB}}{4} - \frac{\chi_{AC}}{2} - \frac{\chi_{BC}}{2} + \frac{1}{4\psi_C N_A} + \frac{1}{4\psi_C N_B} + \frac{1}{2(1-\psi_C)N_C}\right)\eta^2 + \left(\frac{1}{12\psi_c^2 N_A} + \frac{1}{12\psi_c^2 N_B} + \frac{1}{6(1-\psi_c)^2 N_C}\right)\eta^3 \\ & + \left(\frac{1}{24\psi_c^3 N_A} + \frac{1}{24\psi_c^3 N_B} + \frac{1}{12(1-\psi_c)^3 N_C}\right)\eta^4 + \left(-\frac{\chi_{AB}}{4} + \frac{1}{4\psi_c N_A} + \frac{1}{4\psi_c N_A}\right)\phi^2 \\ & + \left(-\frac{1}{12\psi_c^2 N_A} + \frac{1}{12\psi_c^2 N_B}\right)\phi^3 + \left(\frac{1}{24\psi_c^3 N_A} + \frac{1}{24\psi_c^3 N_B}\right)\phi^4 + \left(-\frac{\chi_{AC}}{2} + \frac{\chi_{BC}}{2} + \frac{1}{2\psi_c N_A} - \frac{1}{2\psi_c N_B}\right)\eta\phi \\ & + \left(-\frac{1}{4\psi_c^2 N_A} + \frac{1}{4\psi_c^2 N_B}\right)\eta^2\phi + \left(-\frac{1}{4\psi_c^2 N_A} - \frac{1}{4\psi_c^2 N_B}\right)\eta\phi^2 + \left(\frac{1}{4\psi_c^3 N_A} + \frac{1}{4\psi_c^3 N_B}\right)\eta^2\phi^2 \\ & + \left(\frac{1}{6\psi_c^3 N_A} - \frac{1}{6\psi_c^3 N_B}\right)\eta^3\phi + \left(\frac{1}{6\psi_c^3 N_A} - \frac{1}{6\psi_c^3 N_B}\right)\eta\phi^3. \end{aligned} \tag{2.3}$$

The critical composition ψ_c could be obtained by setting the coefficient of the term of η^3 to zero:

$$\psi_C=\frac{\sqrt{N_C}}{\sqrt{N_A}+\sqrt{N_C}}=1/2;\ N_C=N_A=N_B. \tag{2.4}$$

With $N_C=N_A=N_B=N$, the expansion can be simplified to

$$f_\eta(\eta)=-\frac{1}{2}c_1\eta^2+\frac{1}{4}u_1\eta^4, \tag{2.5}$$

$$f_\phi(\phi)=-\frac{1}{2}c_2\phi^2+\frac{1}{4}u_2\phi^4, \tag{2.6}$$

$$f_{\rm int}(\eta,\phi)=b_1\eta\phi-\frac{b_2}{2}\eta\phi^2+\frac{b_4}{2}\eta^2\phi^2, \tag{2.7}$$

with

$$c_1=-\frac{\chi_{AB}}{2}+\chi_{AC}+\chi_{BC}-\frac{2}{\psi_c N},\quad u_1=\frac{2}{3\psi_c^3 N}, \tag{2.8}$$

$$c_2=\frac{\chi_{AB}}{2}-\frac{1}{\psi_c N},\quad u_2=\frac{1}{3\psi_c^3 N}, \tag{2.9}$$

$$b_1=-\frac{\chi_{AC}}{2}+\frac{\chi_{BC}}{2}, \tag{2.10}$$

$$b_2=\frac{1}{\psi_c^2 N},\quad b_4=\frac{1}{\psi_c^3 N}. \tag{2.11}$$

The constant b_1 reflects the interaction comparison between species C with both A and B; in this work we assume that $b_1=0$. The condition of $b_1=0$ implies that the interaction parameters between C with A and B are the same, i.e., $\chi_{AC}=\chi_{BC}$. The interaction terms in Eq. (2.7) reflect the competition of phase separation between C with A and B. Then, the model free energy for the ternary mixture in terms of η and ϕ is written as

$$F\{\eta,\phi\}=\int dr[f_\eta(\eta)+f_\phi(\phi)+f_{\rm int}(\eta,\phi)]+\frac{D_\eta}{2}\int dr(\nabla\eta(r))^2+\frac{D_\phi}{2}\int dr(\nabla\phi(r))^2, \tag{2.12}$$

where D_η and D_ϕ are phenomenological parameters related to surface energy. For the sake of convenience, functions f_η, f_ϕ and $f_{\rm int}$ are simplified as

$$\frac{df_\eta}{d\eta}=A_\eta\tanh\ \eta-\eta,\qquad \frac{df_\phi}{d\phi}=A_\eta\tanh\ \phi-\phi. \tag{2.13}$$

In the above equations, $A_\eta-1=c_1$ and $A_\phi-1=c_2$. A_ϕ and A_η are phenomenological parameters which are inversely proportional to temperature.

The kinetic equations describing the evolution of the order parameters of a ternary phase separation mixture (A, B, and C) coupled with reversible chemical reaction between A and B can be written as a modified TDGL equation

$$\frac{\partial\eta}{\partial t}=\nabla^2\frac{\delta F\{\eta,\phi\}}{\delta\eta},$$
$$\frac{\partial\phi}{\partial t}=\nabla^2\frac{\delta F\{\eta,\phi\}}{\delta\phi}-(\Gamma_1+\Gamma_2)\phi-(\Gamma_1-\Gamma_2)\eta-(\Gamma_1-\Gamma_2)\psi_C, \tag{2.14}$$

where M_η and M_ϕ are the mobility coefficients, F denotes the mixing free energy of the system. The terms involved with reaction-rate constants in the right-hand side of the second equation in Eq. (2.14) represent reversible reaction kinetics. Using the above free-energy functional F defined in Eq. (2.12), the CDS corresponding to the above TDGL equations is written as

$$\eta(r,t+1)=\eta(r,t)+\langle\langle J_\eta(r,t)\rangle\rangle-J_\eta(r,t),$$
$$\phi(r,t+1)=\phi(r,t)+\langle\langle J_\phi(r,t)\rangle\rangle-J_\phi(r,t)-(\Gamma_1+\Gamma_2)\phi-(\Gamma_1-\Gamma_2)\eta-(\Gamma_1-\Gamma_2)\psi_C,$$
$$J_\eta(r,t)=-D_\eta(\langle\langle\eta\rangle\rangle-\eta)-A_\eta\tanh\ \eta+\eta+b_1\phi-\frac{1}{2}b_2\phi^2+b_4\eta\phi^2,$$
$$J_\phi(r,t)=-D_\phi(\langle\langle\phi\rangle\rangle-\phi)-A_\phi\tanh\ \phi+\phi+b_1\eta-b_2\eta\phi+b_4\eta^2\phi. \tag{2.15}$$

The simulations of the model system are carried out in two-dimensional space with $L\times L=256\times256$ square cells with periodic boundary conditions in both directions. In CDS, $\langle\langle X\rangle\rangle$ is defined as the sum of the nearest neighbors (*NN*) of X and the next nearest neighbors (*NNN*) of X,

$$\langle\langle X\rangle\rangle=\frac{1}{6}\sum_{NN}X+\frac{1}{12}\sum_{NNN}X. \tag{2.16}$$

In the cell dynamic simulations, we set $M_\eta=M_\phi=1.0$, $D_\eta=D_\phi=0.5$, $\psi_c=0.5$, $b_1=0$, $b_2=0.3$, $b_4=0.3/\psi_c$, $A_\phi=A_\eta=1.2$. We should mention that, for the given kinetic rate constants of Γ_1,Γ_2, the equilibrated concentrations of A, B, and C can be calculated according to the following equations:

$$\langle\varphi_A\rangle_e+\langle\varphi_B\rangle_e=1-\langle\varphi_C\rangle,\quad \Gamma_1^*\langle\varphi_A\rangle_e=\Gamma_2^*\langle\varphi_B\rangle_e, \tag{2.17}$$

which affords $\langle\varphi_A\rangle_e=\Gamma_2[1-\langle\varphi_C\rangle]/(\Gamma_1+\Gamma_2)$ and $\langle\varphi_B\rangle_e=\Gamma_1[1-\langle\varphi_C\rangle]/(\Gamma_1+\Gamma_2)$.

As pointed out in the introduction section, in phase separation of binary mixture coupled with reversible reaction, the equilibrium-averaged local volume fractions $\langle\varphi_A\rangle_e,\langle\varphi_B\rangle_e$ do not have to be the same as the initial averaged local volume fractions $\langle\varphi_A\rangle_{\rm initial},\langle\varphi_B\rangle_{\rm initial}$. The relaxation from the initial compositions to equilibrium compositions in our present study can be analytically expressed by solving the second differential equation in Eq. (2.14), neglecting the gradient of chemical potential term. The resulting dynamical equation of the average volume fraction of A is

$$\langle \varphi_A(t)\rangle = \frac{\Gamma_2[1-\langle\varphi_C\rangle]}{\Gamma_1+\Gamma_2} + \left[\langle\varphi_A\rangle_{\text{initial}} - \frac{\Gamma_2[1-\langle\varphi_C\rangle]}{\Gamma_1+\Gamma_2}\right] \times \exp\{-(\Gamma_1+\Gamma_2)t\}. \tag{2.18}$$

For phase-separation dynamics of ternary mixture (A, B, C) coupled with reversible reaction between A and B ($\Gamma_1+\Gamma_2=\Gamma$), linearization of Eq. (2.14) at $\phi=0, \eta=0$ states in Fourier space results in the following coupled first-order differential equations for the fluctuations, $\delta\phi_k, \delta\eta_k$, in the order parameters:

$$\frac{\partial\delta\phi_k}{\partial t} = [(A_\phi-1)k^2 - D_\phi k^4 - (\Gamma_1+\Gamma_2)]\delta\phi_k + [-b_1k^2-(\Gamma_1-\Gamma_2)]\delta\eta_k, \tag{2.19}$$

$$\frac{\partial\delta\eta_k}{\partial t} = [-b_1k^2]\delta\phi_k + [(A_\eta-1)k^2 - D_\eta k^4]\delta\eta_k. \tag{2.20}$$

$\delta\phi_k$ and $\delta\eta_k$ can be expressed as

$$\delta\phi_k = C_1\exp(\lambda_1 t) + C_2\exp(\lambda_2 t),$$
$$\delta\eta_k = C_3\exp(\lambda_1 t) + C_4\exp(\lambda_2 t). \tag{2.21}$$

$C_i (i=1, 2, 3 \text{ or } 4)$ are determined by initial conditions. λ_1 and λ_2 can be solved via eigenvalue problem:

$$\begin{vmatrix} A-\lambda & B \\ C & D-\lambda \end{vmatrix} = 0, \tag{2.22}$$

where A, B, C and D are respectively:

$$A=[(A_\phi-1)k^2 - D_\phi k^4 - (\Gamma_1+\Gamma_2)]$$
$$B=[-b_1k^2-(\Gamma_1-\Gamma_2)],$$
$$C=-b_1k^2, \tag{2.23}$$
$$D=[(A_\eta-1)k^2 - D_\eta k^4],$$

$$\lambda_{1,2} = \frac{A+D}{2} \pm \frac{\sqrt{(A-D)^2+4BC}}{2}. \tag{2.24}$$

Then

$$\lambda_{1,2} = \frac{(A_\phi+A_\eta-2)k^2-(D_\phi+D_\eta)k^4-(\Gamma_1+\Gamma_2)}{2} \pm \frac{\sqrt{[(A_\phi-A_\eta)k^2-(D_\phi-D_\eta)k^4-(\Gamma_1+\Gamma_2)]^2+4b_1k^2[b_1k^2+(\Gamma_1-\Gamma_2)]}}{2}. \tag{2.25}$$

In our present study, where $b_1=0$ and $\Gamma_1=\Gamma_2$, we obtain the following exponential functions:

$$\delta\phi_k = \delta\phi_k(0)\exp[-\gamma_k(\Gamma,k)t], \tag{2.26}$$

$$\delta\eta_k = \delta\eta_k(0)\exp[-\gamma'_k(k)t], \tag{2.27}$$

with

$$\gamma_k(\Gamma,k) = D_\phi k^4 - (A_\phi-1)k^2 + \Gamma, \tag{2.28}$$

$$\gamma'_k(k) = D_\eta k^4 - (A_\eta-1)k^2. \tag{2.29}$$

Since only k modes with positive $\gamma_k(\Gamma)$ are damping, the roots

$$k_\mp = \{(1/2D_\phi)[(A_\phi-1) \mp \sqrt{(A_\phi-1)^2-4D_\phi\Gamma}]\}^{1/2} \tag{2.30}$$

define the upper and lower cutoff wavelengths for the unstable k modes in order parameter ϕ, with

$$(A_\phi-1)^2 - 4D_\phi\Gamma \geqslant 0. \tag{2.31}$$

The effect of upper cutoff wavelength is to dampen the soft modes, thus prevent the continuing domain coarsening and result in microphase separation between A and B. On the other hand, for the case of $b_1=0$ and $\Gamma_1=\Gamma_2$, there only exists lower cutoff wavelength for unstable k modes of order parameter η, therefore, the phase separation between A, B, and C continuously evolves, which results in macrophase separation between A, B, and C. In present study, with $A=A_\phi=A_\eta=1.2$, $D=D_\phi=D_\eta=0.5$, the upper limit of reaction rate constants for the existence of microphase separation can be derived by setting Eq. (2.31) to zero, which affords $\Gamma_{\max}=0.02$.

In this simulation, the forward and backward reaction rate constants are set below 0.01, the averaged initial local volume fractions of the ternary mixture are set at various values. Initially, the system is assumed to be homogeneous. The system is then quenched to unstable phase region to initiate phase separation of the ternary mixture. Due to the change of the local concentrations of species, chemical reaction simultaneously takes place in order to establish equilibrium.

III. RESULTS AND DISCUSSION

The time-dependent Ginzburg–Landau (TDGL) equations for the phase-separation dynamics of ternary mixture (A, B, and C) coupled with reversible chemical reaction between A and B are shown in Eq. (2.14). The η term on the right-hand side of the second equation in Eq. (2.14) can be eliminated by the following change of variables:

$$\phi' = \frac{2\Gamma_1}{\Gamma_1+\Gamma_2}\varphi_A - \frac{2\Gamma_2}{\Gamma_1+\Gamma_2}\varphi_B,$$
$$\eta' = \varphi_A + \varphi_B - \psi_C. \tag{3.1}$$

Then, Eq. (2.14) can be rewritten as

$$\frac{\partial \eta'}{\partial t} = \nabla^2 \frac{\delta F\{\eta', \phi'\}}{\delta \eta'},$$
$$\frac{\partial \phi'}{\partial t} = \nabla^2 \frac{\delta F\{\eta', \phi'\}}{\delta \phi'} - (\Gamma_1 + \Gamma_2)\left[\phi' - \left(\frac{\Gamma_2 - \Gamma_1}{\Gamma_1 + \Gamma_2}\right)\psi_C\right]. \tag{3.2}$$

The reaction term in Eq. (3.2) can be absorbed into the free-energy functional, resulting in the following expression:

$$\frac{\partial \eta'}{\partial t} = \nabla^2 \frac{\delta F'\{\eta', \phi'\}}{\delta \eta'},$$
$$\frac{\partial \phi'}{\partial t} = \nabla^2 \frac{\delta F'\{\eta', \phi'\}}{\delta \phi'}, \tag{3.3}$$

where

$$F'\{\phi', \eta'\} = F\{\phi', \eta'\} + \frac{\alpha}{2}\int dr \int dr' G(r - r') \times [\phi'(r) - \overline{\phi'}][\phi'(r') - \overline{\phi'}]. \tag{3.4}$$

In Eq. (3.4), $G(r-r')$ is the Green's function defined as

$$-\nabla^2 G(r - r') = \delta(r - r'), \tag{3.5}$$

and α and $\overline{\phi'}$ are defined as

$$\alpha = \Gamma_1 + \Gamma_2,$$
$$\overline{\phi'} = \left(\frac{\Gamma_2 - \Gamma_1}{\Gamma_1 + \Gamma_2}\right)\psi_C. \tag{3.6}$$

The free-energy functional form of the above TDGL equation for describing the phase-separation dynamics of ternary mixture (A, B, and C) coupled with reversible chemical reaction between A and B is similar to that of mixture composed of a block copolymer of type A-B and a homopolymer of C.[25] The phase-separation dynamics of the mixture consisting of block copolymer A-B and homopolymer C has been studied by Ito, *et al.*[25,26] The focus of the present study is on the distinctive features of the influence of chemical reaction on phase separation. Namely, we are interested in the effects of concentration relaxation from initial to equilibrium state, as well as chemical reaction lagging behind phase separation upon phase-separation dynamics.

A. Morphological evolution of chemical reaction and phase separation taking place simultaneously

We examined the phase-separation dynamics in cases of $\langle \varphi_i \rangle_{\text{initial}} \neq \langle \varphi_i \rangle_{\text{equilibrium}}$, $(i = \text{A, B})$, as well as different magnitudes of the reaction rate constants Γ. The domain patterns in the cases of $\langle \varphi_A \rangle_{\text{initial}} = 0.3$, $\langle \varphi_B \rangle_{\text{initial}} = 0.1$, $\Gamma_1 = \Gamma_2 = 0.001$ and $\langle \varphi_A \rangle_{\text{initial}} = 0.3$, $\langle \varphi_B \rangle_{\text{initial}} = 0.1$, $\Gamma_1 = \Gamma_2 = 0.0001$ are shown in Fig. 1 and Fig. 2, respectively. It can be seen that lamellar patterns develop in both cases, regardless of $\langle \varphi_i \rangle_{\text{initial}} \neq \langle \varphi_i \rangle_{\text{equilibrium}}$, (i=A, B) and the different magnitudes of reaction rate constants Γ. Please note that the alternating stripes composed of A and B are perpendicular to the interface between microphase-separated domains and macrophase-separated domains. This perpendicular interfacial orientation originates from the fact that both A and B have the same compatibilities towards C, as well as equal equilibrium averaged local volume fractions ($\chi_{AC} = \chi_{BC}$ and $\langle \varphi_A \rangle_{\text{equilibrium}} = \langle \varphi_B \rangle_{\text{equilibrium}} = 0.2$). Concentration relaxation from initial to equilibrium state shows no effect upon phase-separation dynamics in the above cases. Similar to the occurrences of weak-segregation and strong-segregation regimes in large and small α ($\alpha \sim 1/N^2$, where N is the degree of polymerization) in block copolymer system,[27] in Fig. 3, we observed the weak-segregation regime in $\Gamma = \Gamma_1 + \Gamma_2 = 0.002$ and strong-segregation regime in $\Gamma = \Gamma_1 + \Gamma_2 = 0.0002$ ($\alpha \sim \Gamma = \Gamma_1 + \Gamma_2$) for cases shown in Figs. 1 and 2, respectively. The sinusoidal and square wave forms of the order parameter correspond to weak-segregation and strong-segregation regimes, respectively. The domain size of the lamellar thickness can be approximated by the periodicity of either the sinusoidal or the square waves. In present 256 $\times$256 lattice sites simulation, the lamellar thickness in cases of $\Gamma = \Gamma_1 + \Gamma_2 = 0.002$ and $\Gamma = \Gamma_1 + \Gamma_2 = 0.0002$ are approximately 14 and 23 lattice sites, respectively. The ratio of the

FIG. 1. Domain patterns at time step 99 501 for the case of $\langle \varphi_A \rangle_{\text{initial}} = 0.3$, $\langle \varphi_B \rangle_{\text{initial}} = 0.1$, $\Gamma_1 = \Gamma_2 = 0.001$. The model parameters are: $M_\phi = M_\eta = 1$, $D_\phi = D_\eta = 0.5$, $\psi_c = 0.5$, $A_\phi = A_\eta = 1.2$. The interaction parameters are: $b_1 = 0$, $b_2 = 0.3$, $b_4 = 0.3/\psi_c$. The left column displays the concentration profile of species A, in which white and dark regions correspond to high and low concentrations, respectively. The middle and right columns display the concentration profile of B and C, in which white and dark regions correspond to high and low concentrations, respectively.

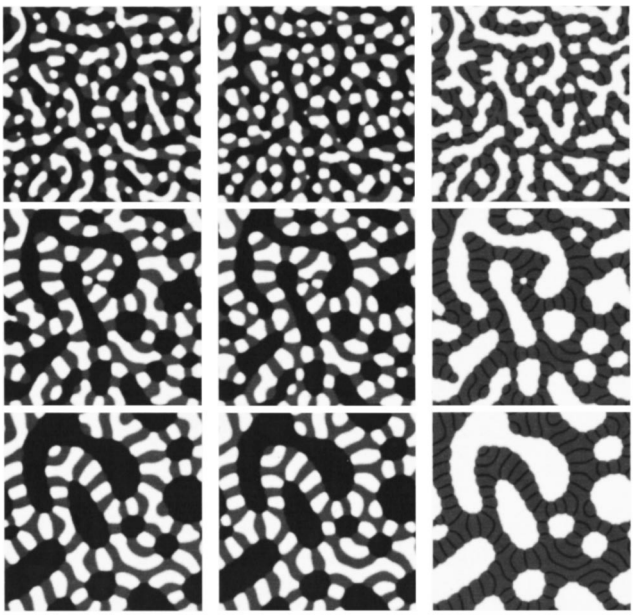

FIG. 2. Time evolution of domain patterns (from top to bottom: time steps are: 19 501, 99 501 and 499 501). The parameters are identical to those in Fig. 1 except $\Gamma_1 = \Gamma_2 = 0.0001$, $\langle \varphi_A \rangle_{\text{initial}} = 0.3$, $\langle \varphi_B \rangle_{\text{initial}} = 0.1$.

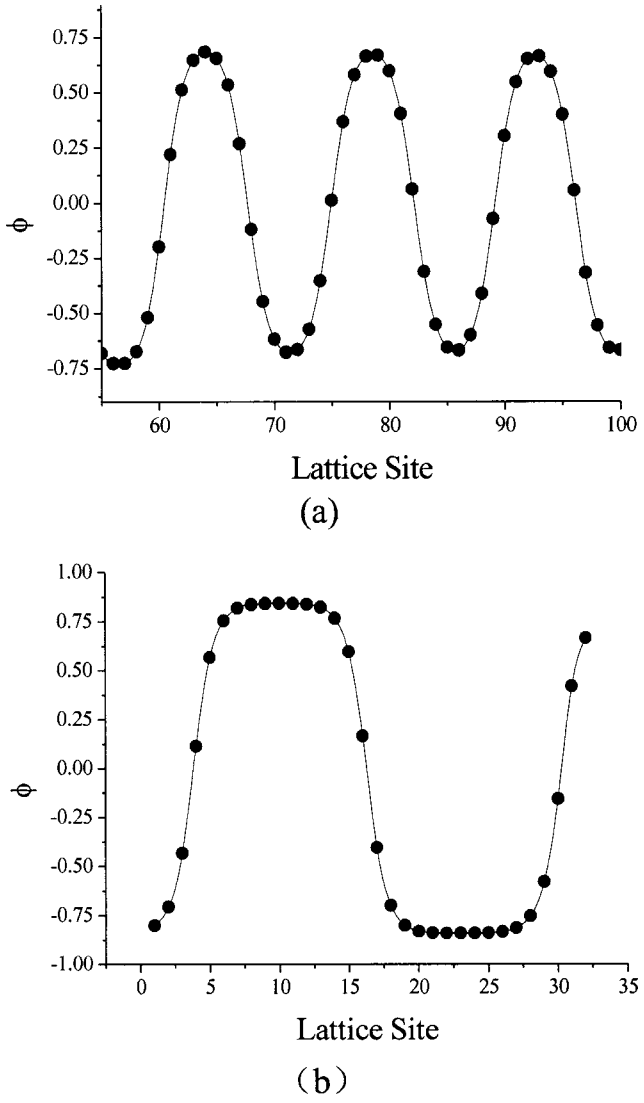

FIG. 3. (a) and (b) displays the profiles of order parameter at time step 99 501 shown in Fig. 1 and time step 499 501 shown in Fig. 2, respectively.

lamellar thickness at these two rate constants is about 1.6. Theoretical studies reveal that for block copolymer, the lamellar thickness of the final equilibrium pattern scales with the molecular weight as a power law $\lambda_L \sim N^{\theta}$. The exponent θ takes the value of 1/2 in the weak-segregation regime and 2/3 in the strong-segregation regime, respectively.[27] In terms of long-range interaction parameter α, lamellar thickness should scale with α as $\lambda_L \sim \alpha^{-1/4}$ or $\lambda_L \sim \alpha^{-1/3}$ in weak or strong segregation regimes. Simulation work on phase separation of binary mixture coupled with reversible reaction reveals that the lamellar thickness scales with the reaction rate constant as $\lambda_L \sim \alpha^{-1/4}$ or $\lambda_L \sim \alpha^{-1/3}$ for high or low reaction rate.[18] However, for phase separation of ternary mixture coupled with reversible chemical reaction, our simulation results suggest a scaling law of the lamellar thickness of the equilibrium pattern with respect to the reaction rate constant different from that observed in binary mixture coupled with reversible chemical reaction, which is shown Fig. 4, where $\langle \varphi_A \rangle_{\text{initial}} = \langle \varphi_B \rangle_{\text{initial}} = 0.2$ and $\Gamma_1 = \Gamma_2$. The lamellar thickness is inversely proportional to $k^1(t)$, where

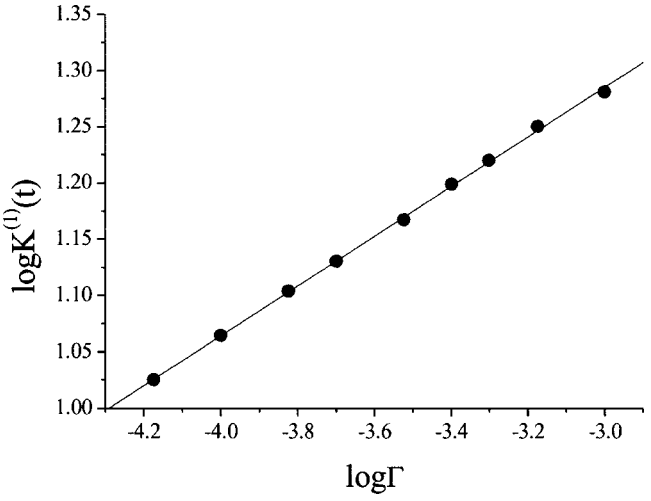

FIG. 4. Scaling law of lamellar thickness with respect to the reaction rate constant in weak and strong segregation regimes. The plot is in double logarithm scale. The X-axis and Y-axis represent the reaction rate constants and the first moment, respectively.

$$k^1(t) = \sum k \cdot S(k,t) / \sum S(k,t)$$

is the first moment of the circularly averaged structure factor $S(k,t)$. In Fig. 4, the first moment is averaged over five random initial conditions. It can be seen from Fig. 4, the lamellar thickness scales with the reaction rate constant as a single power law $\lambda_L \sim \Gamma^{-0.22}$, regardless of high or low reaction rate regimes. This different scaling behavior is presumably due to the influence of species C upon the microphase separation between A and B. It should be pointed out, although the linearization analysis at the early stage of phase separation affords the maximum reaction rate constant for the existence of microphase separation between A and B as $\Gamma = \Gamma_1 + \Gamma_2 = 0.02$, as phase separation further evolves, the microphase separation between A and B is suppressed by the phase separation between C and A and B, and A, B tend to mix with each other, as shown in Fig. 5 for $\Gamma = \Gamma_1 + \Gamma_2 = 0.004$. Therefore, a much smaller mixing effect of chemical reaction is permissible in this ternary mixture system. An interesting feature in Fig. 5 is that in the late stage of phase

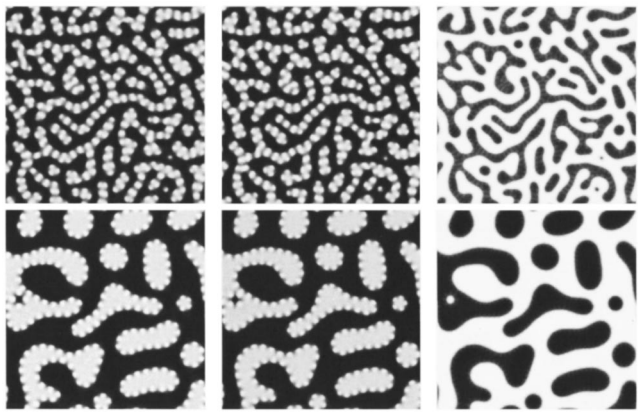

FIG. 5. Domain patterns at time step of 9501 (top) and 99 501(bottom) for the case of $\Gamma_1 = \Gamma_2 = 0.002$. Other parameters are identical to those in Fig. 1.

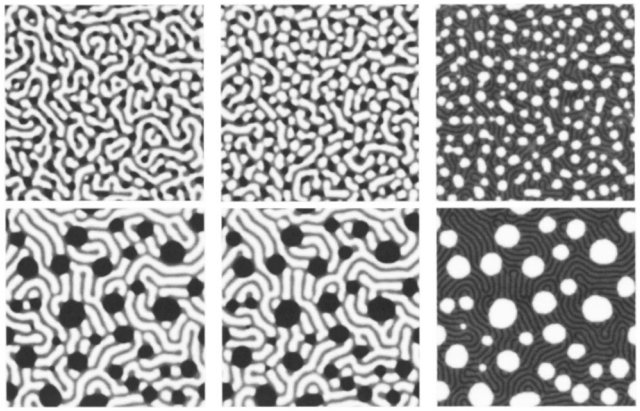

FIG. 6. Domain patterns at time step 4501 and 99 501 for the case of $\langle\varphi_A\rangle_{\text{initial}}=0.5$, $\langle\varphi_B\rangle_{\text{initial}}=0.2$, $\Gamma_1=\Gamma_2=0.001$, where chemical reaction and phase separation take place simultaneously. Other parameters are identical to those in Fig. 1.

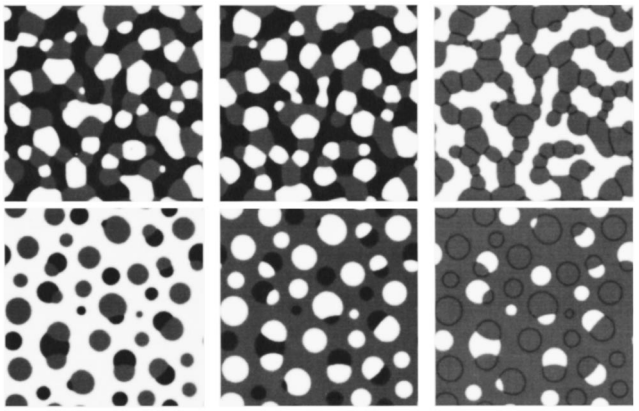

FIG. 8. Domain patterns of phase separation of ternary mixture without the involvement of chemical reaction. The upper row displays the domain patterns at time step 99 501 for the case of $\langle\varphi_A\rangle_{\text{initial}}=\langle\varphi_B\rangle_{\text{initial}}=0.2$. The lower row displays the domain patterns at time step 149 501 for the case of $\langle\varphi_A\rangle_{\text{initial}}=0.5$, $\langle\varphi_B\rangle_{\text{initial}}=0.2$. Other parameters are identical to those in Fig. 1.

separation, species A and B are completely mixed with each other in the interior of the domains composed of A and B, while in the interface between A/B-rich domains and C-rich domains, A and B are phase-separated. In our present study, the maximum rate constant for the existence of microphase separation between A and B at late stage of phase separation is around $\Gamma=\Gamma_1+\Gamma_2=0.002$. The ratio 1.6 obtained from our direct visualization of the lamellar thickness in Fig. 1 and Fig. 2, where Γ is 0.002 and 0.0002, respectively, agrees with the ratio predicted by the scaling law quite well $(10^{0.22})$.

We observed the effect of concentration relaxation from initial to equilibrium state upon phase-separation dynamics in the cases of $\langle\varphi_A\rangle_{\text{initial}}=0.5$, $\langle\varphi_B\rangle_{\text{initial}}=0.2$, $\Gamma_1=\Gamma_2=0.001$ and $\langle\varphi_A\rangle_{\text{initial}}=0.5$, $\langle\varphi_B\rangle_{\text{initial}}=0.2$, $\Gamma_1=\Gamma_2=0.0001$, which are shown in Fig. 6 and Fig. 7, respectively. As shown in Fig. 8, for the case of $\langle\varphi_A\rangle_{\text{initial}}=0.5$, $\langle\varphi_B\rangle_{\text{initial}}=0.2$ without reversible chemical reaction, in the late stage of phase evolution, species A forms the continuous phase. Whereas for the case of $\langle\varphi_A\rangle_{\text{initial}}=0.3$, $\langle\varphi_B\rangle_{\text{initial}}=0.1$ without chemical reaction, no continuous phase exists and isolated A, B, and C domains of irregular shapes fill the whole system.

The dynamics of concentration relaxation from initial to equilibrium state can be described by Eq. (2.18). The plots in Fig. 9 are simulation results, which are identical to the plotting of Eq. (2.18). For $\Gamma=0.002$, it can be seen from Fig. 9 that A and B approach to their equilibrium concentrations at about 2000 time step, which is in the early stage of phase separation. It can also be seen in Fig. 6 that at time step of 4501, due to the rapid decrease of its volume fraction, domains composed of A have already broken up and isolated A and B domains are formed. At the late stage of phase evolution, A and B eventually form lamellar patterns, and the lamellar patterns are perforated by droplets of C. For $\Gamma=0.0002$, the concentration relaxation is much slower than that for $\Gamma=0.002$. From Fig. 9, it can be seen that A and B approach to their equilibrium concentrations at about 25 000 time steps. In this smaller Γ case, at the early and intermediate stage of phase separation, the decrease of the averaged local volume fraction of A is accompanied by the gradual coarsening of the domains. As phase separation further evolves, the domain walls become quite robust, which resist the breakup of the continuous phase composed of A due to the decrease of its volume fraction. Therefore, different domain patterns at lower reaction rate constant are observed. Please note that thickness of the domain walls composed of A and the sizes of dispersed B domains are comparable with those in domain patterns at time step of 99 501 shown in Fig. 2.

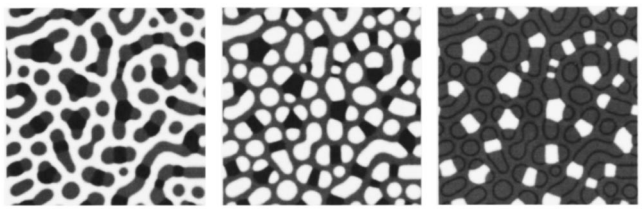

FIG. 7. Domain patterns at time step 99 501 for the case of $\Gamma_1=\Gamma_2=0.0001$. Other parameters are identical to those in Fig. 6.

B. Chemical reaction lagging behind phase separation

Another distinctive feature of phase separation coupled with reversible chemical reaction is that the chemical reaction could be turned on after phase separation has proceeded for finite time steps, which finds no correspondence in phase separation of block copolymer.

In the present study, we let the phase separation for the case of $\langle\varphi_A\rangle_{\text{initial}}=0.5$, $\langle\varphi_B\rangle_{\text{initial}}=0.2$ proceed for 1.5×10^5 time steps without the involvement of chemical reaction. The resulting domain patterns are shown in Fig. 8. Chemical reaction is then turned on and we observed different domain evolution patterns for different reaction rate constants $\Gamma=0.002$ and $\Gamma=0.0002$. Figure 10 displays the domain patterns for the case of $\Gamma=0.002$. As shown at time step of 150 501 in Fig. 10, species A emerges inside the droplets of

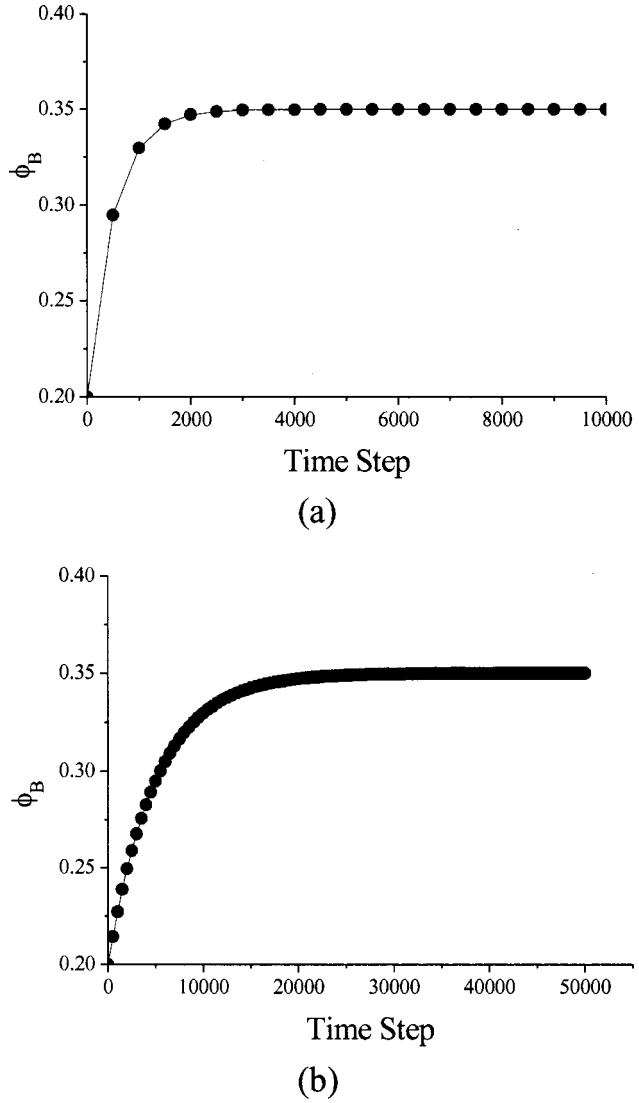

FIG. 9. Concentration relaxation profiles for the cases of $\Gamma_1=\Gamma_2=0.001$ and $\gamma_1=\Gamma_2=0.0001$ are displayed in (a) and (b), respectively.

B and forms concentric pattern. On the other hand, species B emerges as either small droplets or stripes inside A-rich domains. As chemical reaction coupled phase separation further evolves, lamellar domain patterns gradually emerge and domains are coarsening. The domain patterns eventually transform into lamellar patterns similar to those shown in Fig. 6.

Different domain patterns are observed for the case of smaller reaction rate constants $\Gamma=0.0002$, which are shown in Fig. 11. As shown at time step 150 501 in Fig. 11, no appreciable change of domain patterns could be observed. As the phase separation evolves, the continuous domain composed of A gradually shrinks and dispersed B domains grow in size due to the conversion from A to B. As shown at time step 189 501, the initially smaller B domains have grown considerably. It can also be seen from Fig. 11 that dispersed B domains are compressed and deformed from initially circular shapes. The origin of the different domain pattern formations observed in the cases with different reaction rate constants $\Gamma=0.002$, $\Gamma=0.0002$ can be explained in terms of the discrepancy between the domain sizes at the time step

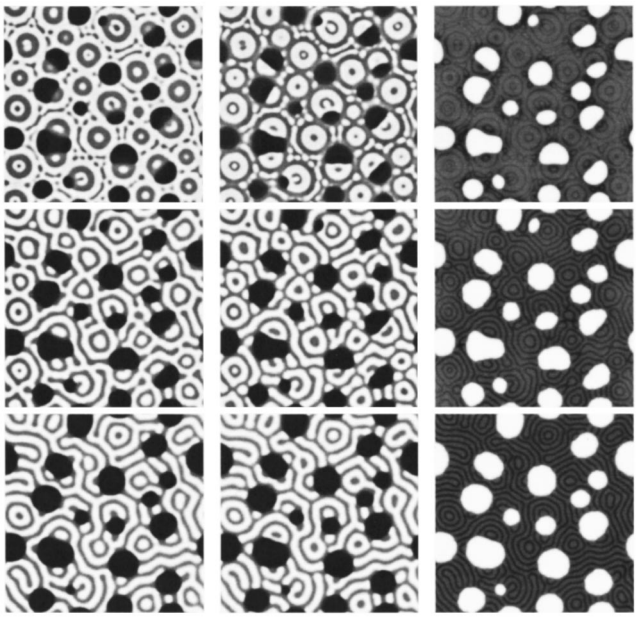

FIG. 10. Domain patterns at time steps 150 501, 154 501, and 199 501 for chemical reaction lagging behind phase separation by 1.5×10^5 time steps for the case of $\Gamma_1=\Gamma_2=0.001$, $\langle\varphi_A\rangle_{\text{initial}}=0.5$, $\langle\varphi_B\rangle_{\text{initial}}=0.2$. Other parameters are identical to those in Fig. 1.

immediately before the turning on of the chemical reaction and the inherent lamellar thickness determined by the magnitude of the reaction rate constants. For $\Gamma=0.002$, the inherent lamellar thickness can be approximated from the order parameter profile shown in Fig. 12, which is obtained from Fig. 6 by visual inspection and plotting of the order parameter with respect to lattice sites. The lamellar thickness is the same as the periodicity of the sinusoidal wave, which is about 14 lattice sites. Although the domain size distribution of dispersed B phase at time step 149 501 in Fig. 8 is not uniform, the domain sizes of most of the isolated B droplets are comparable and larger than the inherent lamellar thickness, which is about 14 lattice sites as shown in Fig. 12. The profile in its local volume fraction of the largest B droplet is shown in Fig. 12, and can be used to approximate the domain

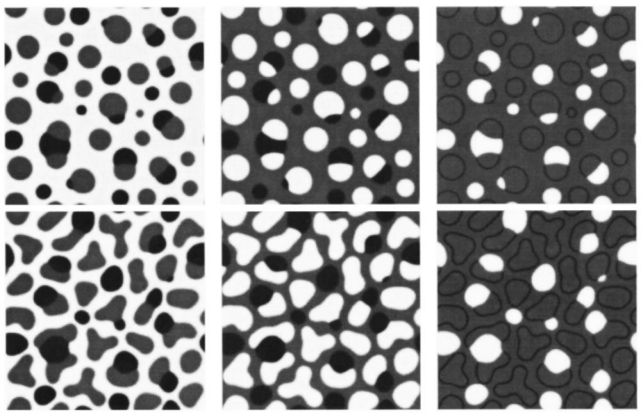

FIG. 11. Domain patterns at time steps 150 501 and 189 501 for chemical reaction lagging behind phase separation by 1.5×10^5 time steps for the case of $\Gamma_1=\Gamma_2=0.0001$, $\langle\varphi_A\rangle_{\text{initial}}=0.5$, $\langle\varphi_B\rangle_{\text{initial}}=0.2$. Other parameters are identical to those in Fig. 1.

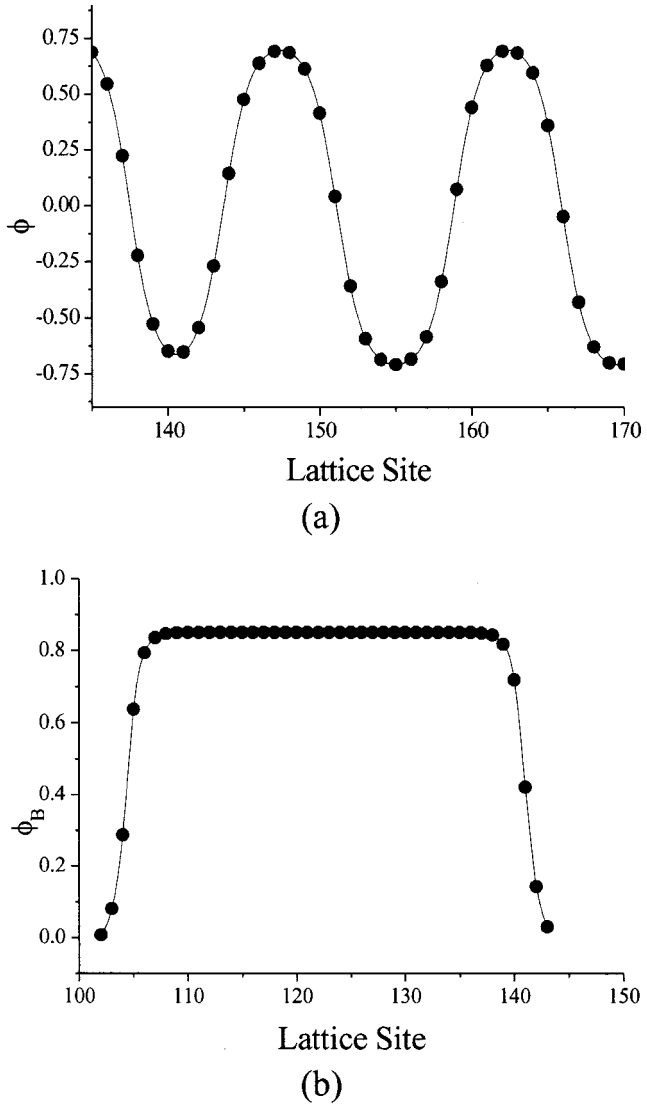

FIG. 12. (a) displays the order parameter profile at time step 99 501 shown in Fig. 6. (b) displays the local volume fraction profile of the biggest droplet rich in B at time step 149 501 shown in Fig. 8 for $\langle \varphi_A \rangle_{\text{initial}} = 0.5$, $\langle \varphi_B \rangle_{\text{initial}} = 0.2$.

size of the largest droplet rich in B. The diameter of the biggest droplet is evaluated at the half height of the square wave, which is about 37 lattice sizes. Thus the radii of the biggest droplet rich in phase B is about 19 lattice sites. Obviously, for the case of turning on the reaction with rate constant of $\Gamma = 0.002$ after 1.5×10^5 time steps of phase separation evolution, the domain sizes of most of the dispersed B domains exceed the inherent lamellar thickness, which triggers the emergence of circular A domains inside the B domains. Also, by visual inspection, most of the gaps rich in A between adjacent dispersed B and C domains exceed the inherent lamellar thickness, which render the appearance of either small droplets or stripes rich in B inside the continuous phase composed of A. The above consideration in terms of the discrepancy between the domain sizes at the time step immediately before the turning on of the chemical reaction and the inherent lamellar thickness determined by the magnitude of the reaction rate constants also explains the different domain evolution behavior for the case

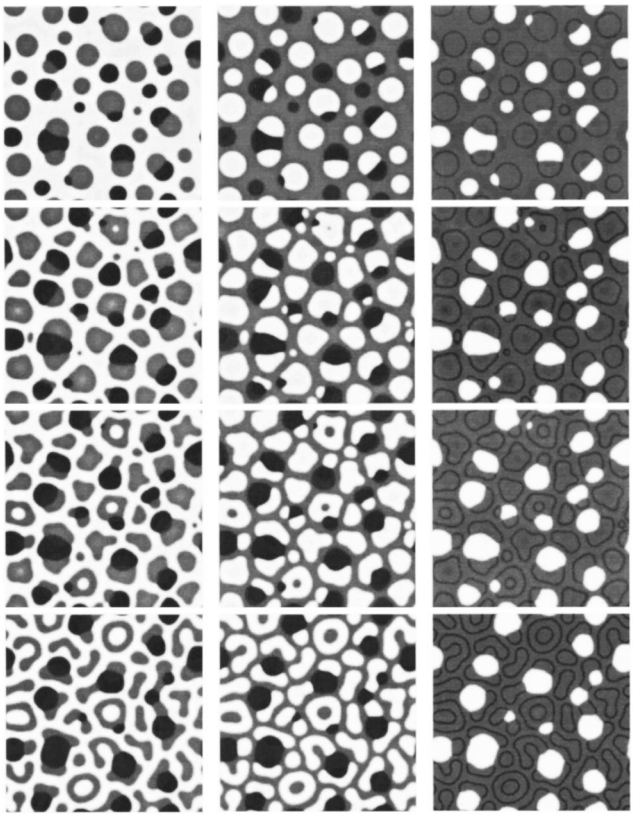

FIG. 13. Domain patterns at time steps 151 001, 155 001, 160 001, and 200 001 from top to bottom for chemical reaction lagging behind phase separation by 1.5×10^5 time steps in the case of $\Gamma_1 = \Gamma_2 = 0.0002$, $\langle \varphi_A \rangle_{\text{initial}} = 0.5$, $\langle \varphi_B \rangle_{\text{initial}} = 0.2$.

of $\Gamma = 0.0002$. Contrary to the case of $\Gamma = 0.002$, in this case, the inherent lamellar thickness far exceeds the radii of the largest B droplets as well as the largest gap rich in A between adjacent B or C domains. It should be pointed out that the inherent lamellar thickness for the case of $\Gamma = 0.0002$ can be approximated by the scale law we discussed in the preceding section. Then, the inherent lamellar thickness for the case of $\Gamma = 0.0002$ should be about 23 ($14 \times 10^{0.22}$) lattice sites. At time step of 189 501 shown in Fig. 11, the domains rich in B are deformed in order to prevent the domain size from exceeding the inherent lamellar thickness.

Slightly different domain patterns from those for $\Gamma_1 = \Gamma_2 = 0.0001$ were observed for $\Gamma_1 = \Gamma_2 = 0.0002$, which are shown Fig. 13. The inherent lamellar thickness in this case is about 20 lattice sites ($14 \times 5^{0.22}$), which is slightly larger than the radii of the largest B-rich droplet as well as the largest gap rich in A between adjacent B or C droplets at time step 150 K. As shown in Fig. 13, there is no appreciable difference between the domain patterns at time step 151 k and 150 k. Similar to the case for $\Gamma_1 = \Gamma_2 = 0.0001$, neither A emerges inside B-rich droplets nor B emerges inside A-rich gaps at time step 151 k. Due to chemical conversion of A to B, B-rich domains expand while the A-rich domains shrink. The expansion of the B-rich domains is accompanied by their deformation, which tends to reduce their domain sizes. As shown in time steps 155 k and 160 k, Species A emerges inside several deformed B-rich droplets due to the fact that

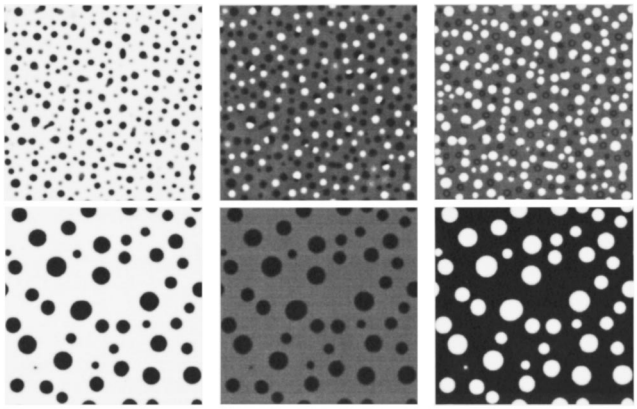

FIG. 14. Domain patterns at time step 4501 and 49 501 for the case of $\langle\varphi_A\rangle_{\text{initial}}=0.5$, $\langle\varphi_B\rangle_{\text{initial}}=0.2$, $\Gamma_1=0.0001$, $\Gamma_2=0.0006$, where chemical reaction and phase separation take place simultaneously.

their sizes exceed the inherent lamellar thickness. Because the lamellar thickness is only slightly larger than the domain sizes of these B-rich droplets before the turning on of the chemical reaction, this transition in domain sizes of B-rich droplets can be achieved much easier than in the case of $\Gamma_1=\Gamma_2=0.0001$. In this case, we observed unique domain patterns originated from the delicate balance of domain expansion and deformation of B-rich phase after the turning on of the chemical reaction.

C. Crossover between different phase regions in the ternary polymeric mixture

A distinction of phase separation of ternary polymeric mixture from binary mixture is the existence of multiple-phase regions in ternary mixture. In the study of symmetric ternary polymeric mixture (same χN, N for the three components) by Huang *et al.*,[22] complicated phase diagrams were constructed at various χN, In these phase diagrams, two or three phases may coexist, depending upon the relative volume fractions of the three constituents. By setting $\langle\varphi_i\rangle_{\text{initial}}\neq\langle\varphi_i\rangle_{\text{equilibrium}}$ ($i=$ A, B), it is possible for the ternary mixture to crossover from one phase region to another along lines parallel to AB side of the triangle phase diagram. This unique feature might offer the possibilities of generating interesting steady-state phase patterns.

Our preliminary studies reveal that indeed, steady-state phase patterns can be observed as shown in Fig. 14. The initial volume fractions are set to $\langle\varphi_A\rangle_{\text{initial}}=0.5$, $\langle\varphi_B\rangle_{\text{initial}}=0.2$ and the equilibrium volume fractions are $\langle\varphi_A\rangle=0.6$, $\langle\varphi_B\rangle=0.1$, which is achieved by set $\Gamma_1=0.0001$, $\Gamma_2=0.0006$. As shown in Fig. 14, the original phase rich in B eventually disappears as its volume fraction is decreased to 0.1 due to conversion to A, and droplets rich in C grow continuously. It should be pointed out that at $\langle\varphi_A\rangle_{\text{initial}}=0.6$, $\langle\varphi_B\rangle_{\text{initial}}=0.1$, and $\Gamma_1=0.0001$, $\Gamma_2=0.0006$, the domain pattern indicates the existence of only one phase rich in A by computer simulation and there is no phase separation between A and C, contrary to the phase separation between A and C shown in Fig. 14. By setting $\langle\varphi_i\rangle_{\text{initial}}\neq\langle\varphi_i\rangle_{\text{equilibrium}}$ ($i=$A, B), we observed kinetically controlled phase evolution in Fig. 14.

IV. CONCLUSION

In this paper, we studied the phase-separation dynamics of a ternary mixture coupled with a reversible chemical reaction between two constituents. We have demonstrated that the TDGL describing the above-mentioned system has similar free-energy functional form to that for describing the phase-separation dynamics of a mixture composed of a homopolymer and a block copolymer. Our simulation study reveals that for the case of equal forward and backward reaction rates, the lamellar thickness scales with the reaction rate constant as a single power law $\lambda_L\sim\Gamma^{-0.22}$, regardless of high or low reaction rate regimes. The emphasis of the present study is on the distinctive features of influence of chemical reaction on phase separation. We investigated the effects of concentration relaxation from initial to equilibrium state, as well as chemical reaction lagging behind phase separation upon phase separation dynamics and observed interesting steady-state pattern formation.

Our studies provide new insight into the origin of the unusual steady-state pattern formation. In the cases of $\langle\varphi_i\rangle_{\text{initial}}\neq\langle\varphi_i\rangle_{\text{equilibrium}}$ ($i=$A, B) and phase separation and chemical reaction taking place simultaneously, unusual steady-state patterns could be observed only when one of the two reactive constituents is the continuous phase in an otherwise unreactive system. At sufficiently small reaction rate constants Γ, the pathway of the breakup of the continuous phase is blocked due to the robustness of the domain walls, which is built-up in a sufficiently long coarsening process.

In the cases where chemical reaction lags behind phase separation, the different pattern evolutions at large and small reaction rate constants can be interpreted in terms of the discrepancy between the domain sizes at the time step immediately before the turning on of the chemical reaction and the inherent lamellar thickness determined by the magnitude of the reaction rate constants. If the domain sizes at the time step immediately before the turning on of the chemical reaction exceed the inherent lamellar thickness, which is determined by the reaction rate constants, domains rich in one reactive phase emerge inside another reactive phase. Also, the counterbalance between the expansion of the minority phase due to the concentration relaxation and its deformation after the turning on of chemical reaction needs to be taken into consideration in the case where the lamellar thickness is only slightly larger than the domain size immediately before the turning on of chemical reaction.

Our preliminary studies also reveal that the crossover of the ternary mixture from one phase region to another along lines parallel to AB side of the triangle phase diagram due to the concentration change between A and B might generate interesting steady-state domain patterns.[28]

In our present study, hydrodynamic effects are neglected. We think that the hydrodynamic effects should not alter the main features in this paper, although hydrodynamic effects will affect the domain growth exponent of macrophase separation between A/B and C.

ACKNOWLEDGMENTS

This work was supported by the Special Funds for Major State Basic Research Projects (G1999064800) and NSFC.

[1] K. Binder and D. Stauffer, Phys. Rev. Lett. **33**, 1006 (1974).
[2] J. D. Gunton, M. San Miguel, and P. S. Sahni, in *Phase Transitions and Critical Phenomena*, edited by C. Domb and J. L. Lebowitz (Academic, London, 1983), Vol. 8.
[3] B. O'Shaughnessy and D. Vavylonis, Macromolecules **32**, 1785 (1999).
[4] B. O'Shaughnessy and U. Sawhney, Macromolecules **29**, 7230 (1996).
[5] S. F. Corberi, G. Gonnella, and A. Lamura, Phys. Rev. Lett. **83**, 4057 (1999).
[6] M. Okada and T. Sakaguchi, Macromolecules **32**, 4154 (1999).
[7] M. D. Smith and P. F. Green, Macromolecules **32**, 8392 (1999).
[8] F. Qiu, H. Zhang, and Y. Yang, J. Chem. Phys. **108**, 9529 (1998).
[9] F. Qiu, H. Zhang, and Y. Yang, J. Chem. Phys. **109**, 1575 (1998).
[10] Z. Zhang, H. Zhang, and Y. Yang, J. Chem. Phys. **118**, 8346 (2000).
[11] Q. Tran-Cong, J. Kawai, Y. Nishikawa, and H. Jinnai, Phys. Rev. E **60**, R1150 (1999).
[12] K. Kataoka, O. Urakawa, H. Nishioka, and Q. Tran-Cong, Macromolecules **31**, 8809 (1998).
[13] Q. Tran-Cong and A. Harada, Phys. Rev. Lett. **76**, 1162 (1996).
[14] A. Harada and Q. Tran-Cong, Macromolecules **30**, 1643 (1997).
[15] B. A. Huberman, J. Phys. Chem. **65**, 2013 (1976).
[16] S. C. Glotzer and A. Coniglio, Phys. Rev. E **50**, 4241 (1994).
[17] S. C. Glotzer, E. A. Di Marzio, and M. Muthukumar, Phys. Rev. Lett. **74**, 2034 (1995).
[18] J. J. Christensen, K. Elder, and H. C. Fogedby, Phys. Rev. E **54**, R2212 (1996).
[19] D. Carati and R. Lefever, Phys. Rev. E **56**, 3127 (1997).
[20] M. Motoyama, J. Phys. Soc. Jpn. **65**, 1894 (1996).
[21] M. Motoyama and T. Ohta, J. Phys. Soc. Jpn. **66**, 2715 (1997).
[22] C. Huang, M. Olvera de la Cruz, and B. W. Swift, Macromolecules **28**, 7996 (1995).
[23] Y. Ma, J. Phys. Soc. Jpn. **69**, 3597 (2000).
[24] M. Ipsen, L. Kramer, and P. G. Sorensen, Phys. Rep. **337**, 193 (2000).
[25] T. Ohta and A. Ito, Phys. Rev. E **52**, 5250 (1995).
[26] A. Ito, Phys. Rev. E **58**, 6158 (1998).
[27] F. Liu and N. Goldenfeld, Phys. Rev. A **39**, 4805 (1989).
[28] B. Liu, C. Tong, and Y. Yang, J. Phys. Chem. B **105**, 10091 (2001).